The Inverted Pendulum

Jeffrey Aguilar,[1] Christopher Marcotte,[2] Gustavo Lee,[3] and Balachandra Suri[2]
[1)] *Woodruff School of Mechanical Engineering, Georgia Institute of Technology, Atlanta, Georgia 30332*
[2)] *School of Physics, Georgia Institute of Technology, Atlanta, Georgia 30332*
[3)] *School of Aerospace Engineering, Georgia Institute of Technology, Atlanta, Georgia 30332*

(Dated: 15 December 2011)

Over the course of a few decades, the pendulum problem has become a prime example in the instruction of many concepts in linear and nonlinear dynamics. Particularly, the inverted pendulum has been illuminating in the areas of dynamical stability and control. Our intent with this dynamics problem was to explore the stability of the inverted state while vertically driving the pivot point. Forcing the pivot with a simple sine wave trajectory, we modified the frequency and amplitude parameters of the forcing to experimentally map its stability boundaries. Within this stable state, we also observed further dynamics of its behaviour such as frequency of oscillation. It was discovered that the frequency was positively correlated with the peak kinetic energy exhibited by the vertical forcing.

I. INTRODUCTION

The inverted pendulum is a classic textbook example that has provided significant insights into stability and control theory for many decades. It was first investigated by P.L. Kapitza, whose interest in the problem can be summarized in the following quote: "the striking and instructive phenomenon of dynamical stability of the turned pendulum not only entered no contemporary handbook on mechanics but is also nearly unknown to the wide circle of specialists... ...not less striking than the spinning top and as instructive."[1]. The important question this problem poses is how one would go about stabilizing the pendulum about the top equilibrium point, which is inherently unstable. This problem has been approached from various perspectives. It has been established that the general three dimensional case is controllable with planar movements (i.e., on a controlled cart)[2], and many of the well-known control methods have been explored for this stabilization strategy, including fuzzy control[3] and neural networks[4]. These planar stabilizing methods (or even single direction horizontal movements) are instructive mainly in applications of control theory. However, stabilizing with a periodic vertical forcing of the pendulum without the use of feedback is much more enlightening from a dynamics perspective. And thus, our intent was to investigate the stabilization of the inverted pendulum through the oscillated vertical driving of the pivot point of the pendulum. There was no constraint on the angles that the rod can travel.

II. THEORY

In our study, we experimented on both the single and to a lesser extent, the double pendulum. We will review the theory for each of these in turn. Figure 1 illustrates the diagram for the theoretical single pendulum.

A. Single Inverted pendulum, N=1

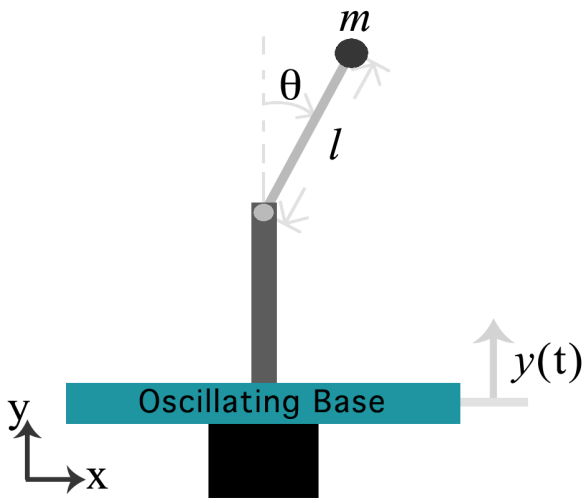

FIG. 1. Single Pendulum Diagram: The oscillating base moves the pivot of the pendulum of length, l, and mass, m. The pendulum, free to rotate about its pivot, has an angular position measured from the inverted point.

The Lagrangian of the inverted pendulum with a vertically driven pivot is as follows:

$$\mathcal{L} = \frac{m}{2}(\ell^2\dot{\theta}^2 + \dot{y}^2 + 2\ell\dot{y}\dot{\theta}\sin\theta) - mg(y(t) + \ell\cos(\theta)) \quad (1)$$

where θ and $\dot{\theta}$ are the angular position and velocity, respectively, g is gravity, ℓ is the rod length, and m is the mass of the pendulum. The driving function, y is the

sinusoid of the following form.

$$y(t) = A\sin(2\pi f t) \tag{2}$$

where A is the forcing amplitude, f is the forcing frequency, and t is time. Equation 1 can be solved using the Euler-Lagrange formalism to yield the following equation of motion.

$$0 = \ddot{\theta} + \gamma\zeta(\dot{\theta}) + (\ddot{y} - \alpha)\sin\theta \tag{3}$$

where $\alpha = (g/l)\omega^2$, $\ddot{y}$ is the second derivative of the vertical driving function, and $\ddot{\theta}$ and $\dot{\theta}$ are the angular acceleration and velocity, respectively. All the values were derived with respect to a dimensionless time, $\tau = \omega t$, with ω being a forcing frequency in rad/s. The damping term, γ is a frictional constant, with $\zeta(\dot{\theta})$ being some function of the velocity. This term was added knowing there was damping in the system. Without yet characterizing the damping, we postulated a frictional model, in which case the ζ function would just be the sign of the velocity[5].

1. *Stability Analysis*

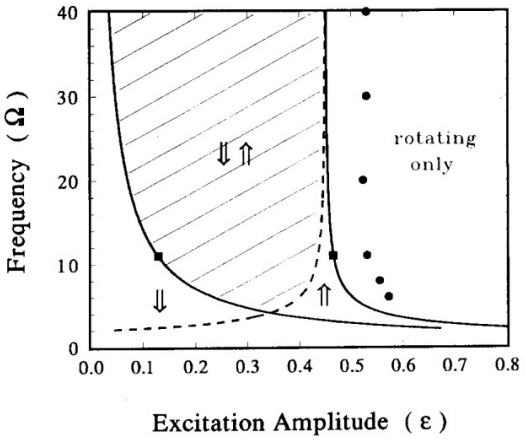

FIG. 2. Stability diagram for the pendulum from Gronbech-Jensen et. al[6]

The fixed points are given by $(\theta*, \dot{\theta}*)_- = (\pi, 0)$ and $(\theta*, \dot{\theta}*)_+ = (0, 0)$. A study on the stability of the inverted state, (0,0), within the forcing frequency/amplitude parameter space has been done in previous literature[6]. It was calculated that the inverted state was stable as long as the frequency and amplitude were within the following two curves:

$$\epsilon = \sqrt{2}/\Omega \tag{4}$$

$$\epsilon = 0.450 + 1.799/\Omega^2 \tag{5}$$

indicated in Figure 2 by the solid lines. The forcing frequency, Ω, and the the forcing amplitude, ϵ, are both reduced units defined by the following equations:

$$\Omega = \frac{f}{f_0} \tag{6}$$

$$\epsilon = \frac{A\omega_0^2}{g} \tag{7}$$

where f is the frequency in Hz, f_0 is the natural frequency of the pendulum, A is the amplitude in meters, ω_0 is the natural frequency in $radians/sec$, and g is gravity in m/s^2.

2. *Effective Energy Potential*

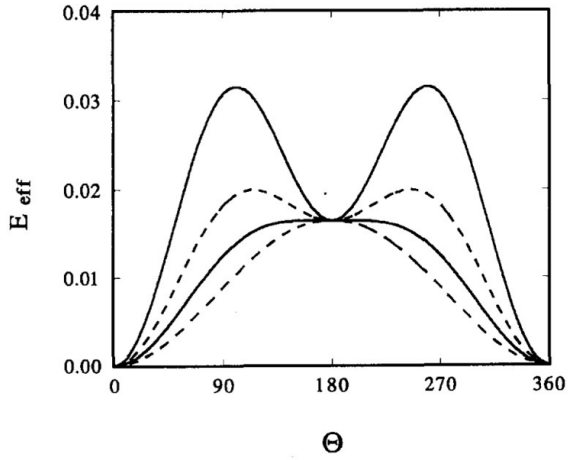

FIG. 3. Effective energy potential versus angular position from Gronbech-Jensen et. al.[6]

The construction of the energy potential for the vertically driven pendulum has also been done in previous literature[6]. Their method for the derivation of this potential function was through the separation of small and large time scales in the angular position:

$$\theta = \Theta + \xi \tag{8}$$

where Θ is the slow overall movement of the pendulum, and ξ indicates the effect of quick local movements due to the shaking. There was also an assumption of small energy losses from damping. Their final approximation was as follows:

$$E_{eff}(\Theta) \approx \frac{1}{\Omega^2}[1 - \cos\Theta + \frac{1}{2}(\frac{\epsilon\Omega}{2})^2(1 - \cos 2\Theta)] \tag{9}$$

As illustrated in Figure 3 for different damping values, when the amplitude ϵ is sufficiently large, a potential well develops at both $\Theta = \pi$, the top fixed point for that paper's convention, and $\Theta = 0$, the bottom fixed point, such that both equilibria are stable.

While reconstructing this potential would be nearly impossible with our data, which more closely behaves with non-negligible frictional damping instead of negligible viscous damping (based on their assumptions), it is still useful to note the phenomenon of this energy well and how it illustrates that the bottom fixed point remains stable when the bifurcation occurs at the inverted state.

B. Double Inverted pendulum, N=2

The double inverted pendulum was also explored near the end of our week experimenting. As such, it was useful to compare how our experimental results compared with a theoretical model. The following equations of motion were painstakingly derived:

$$\ddot{\theta}_1 = -\frac{m_2(L_1\dot{\theta}_1^2\sin(2\theta_1-2\theta_2)+2L_2\dot{\theta}_2^2\sin(\theta_1-\theta_2))+g((2m_1+m_2)\sin(\theta_1)+m_2\sin(\theta_1-2\theta_2))-\ddot{y}((2m_1+m_2)\sin(\theta_1)+m_2\sin(\theta_1-2\theta_2))}{2L_1\big(m_2\sin(\theta_1-\theta_2)^2+m_1\big)}$$

$$\ddot{\theta}_2 = \frac{L_2m_2\dot{\theta}_2^2\sin(2\theta_1-2\theta_2)\ +(m_1+m_2)\big(2L_1\dot{\theta}_1^2\sin(\theta_1-\theta_2)+g(\sin(2\theta_1-\theta_2)-\sin(\theta_2))\big)+\ddot{y}(m_1+m_2)(\sin(\theta_2)-\sin(2\theta_1-\theta_2))}{2L_2\big(m_2\sin(\theta_1-\theta_2)^2+m_1\big)} \quad (10)$$

While it would be especially difficult to make purely analytical calculations, these equations were still useful to numerically integrate for simulation purposes.

C. Simulink

Both the double and single inverted pendulum equations were modeled into Simulink with adjustable parameters for simulation. The particular solver used varied depending on the circumstances, however, the default variable step solver, ODE45, was generally both sufficiently accurate and computationally affordable.

III. METHODS

We experimentally analysed the stability of the inverted equilibrium point. This was done by varying the sinusoidal parameters of the pivot forcing.

A. Materials

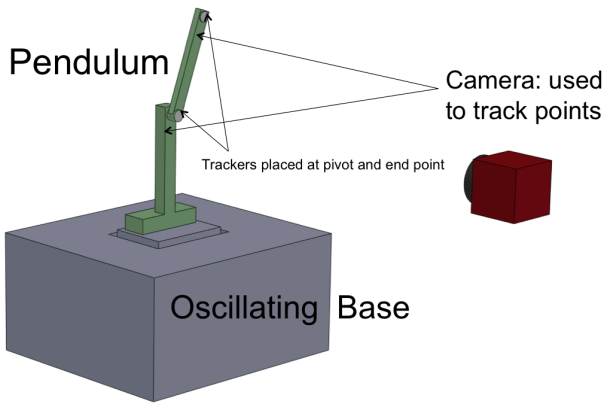

FIG. 4. General experimental set-up

Figure 4 illustrates all of the components used in the experimental set up. The base of the pendulum was rigidly attached to an oscillating base. The pendulum was free to move through its entire range of motion without any constraints. Trackers, either 10 mm white plastic balls or white out on black electrical tape were fastened to the pivot and end of the pendulum for camera tracking purposes.

1. *Oscillating Base*

The oscillating base was the device used to vertically shake the pendulum pivot. It consisted of a function generator, amplifier, motor, air bearing, accelerometer and oscilloscope. The function generator sends the sine wave signal at an adjustable frequency. The signal is then passed through an amplifier with an adjustable current which is what sets the forcing amplitude. This amplified signal is then sent to the motor which converts the current into force. An accelerometer attached to the motor sends a voltage signal to an oscilloscope providing forcing amplitude feedback by a peak-to-peak voltage, V_{pk}, which can be converted to displacement amplitude in meters with the following equation:

$$A_{disp} = \frac{9.8 * V_{pk}/2 * 10}{(2\pi * Frequency)^2} \quad (11)$$

2. *Camera Tracking*

Two cameras were used. The first was a PointGrey high speed camera with a maximum of 200 fps. It employed real-time tracking with LabView software. This made time steps between frames variable and also made tracking points susceptible to being lost with the slightest obscurity of the trackers from the camera's view, such as when we used the double pendulum of equal rod lengths and the second pendulum swung in front of the pivot. Also, spinning modes tended to be too fast to for a 200

fps camera. To fix these problems, we then used a MotionXtra 1000 fps camera that required off-line tracking in Matlab. The following steps are the basic elements of the tracking algorithm employed to track a single point in Matlab:

1. Select search-point coordinates.
2. Threshold data to distinguish tracker pixels from non-tracker pixels.
3. Average all tracker pixel locations for a small area of pixels about the search point to get the actual centroid position.
4. Make centroid the updated search-point for the next frame.

Iteratively repeat steps 2-4 for all frames. This algorithm, also used in the Labview program, has many of the same drawbacks as the real-time scenario, mainly being, that, once a tracker is lost as a result of obscurity, it generally remains lost, and the resulting position data is useless. For the double pendulum example, where the second pendulum would at times obscure the pivot, an assumption was written into Matlab that the pivot only moves in the y direction such that, during times of obscurity, this assumption along with known values such as the location of the first pendulum and the first pendulum's length could be used to accurately determine the pivot's location. Also, certain pendulum movements were too fast even at 1000 fps. Thus, the true advantage of off-line tracking, manual tracking, was also integrated into Matlab.

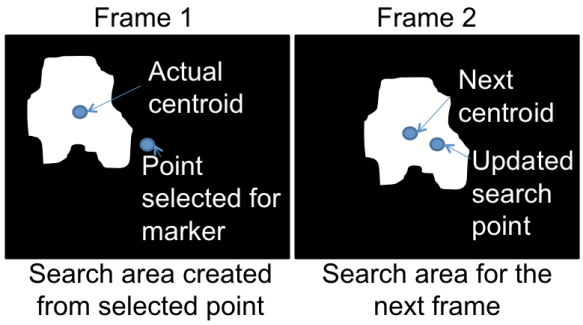

FIG. 5. Illustration of tracking algorithm

3. *Original Pendulum*

The original pendulum was an aluminium pendulum with an effective length of 6.88 cm (see Figure 6). All effective length calculations were roughly estimated as the centroids of the rods. This pendulum had two problems. The first was the small range of available frequencies for the stability mapping experiment about the inverted point. This was due to the shaker's stroke and power constraints as well as the rod's length. The second was a strange frictional issue with the bearing itself that caused the pendulum to randomly settle off-axis of either fixed point (see Figure 7).

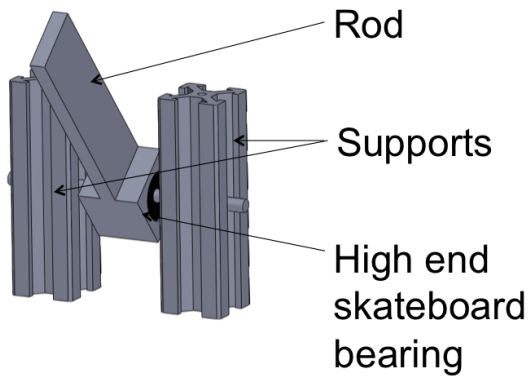

FIG. 6. Original pendulum

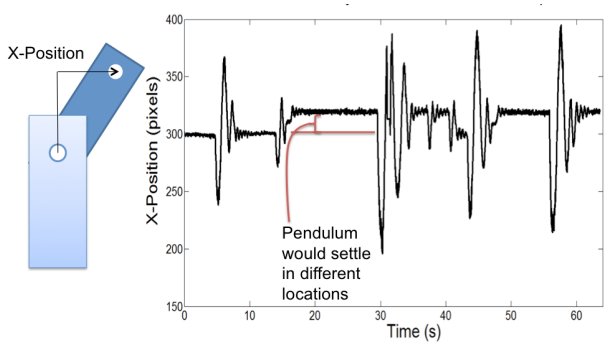

FIG. 7. Illustration of frictional issue. Pivot forced vertically at 22 Hz and about 7 mm amplitude

4. *Modified Pendulum*

This pendulum was a modified version of the original pendulum as a solution to the original pendulum's problems, with a shorter length of 3.13 cm (see Figure 8). The high end skate bearing was actually comprised of two separate ball bearings. Removing one of them significantly improved the strange frictional issue, with the pendulum more consistently settling at the actual fixed points. This was our main pendulum.

In characterizing the decay of the system, we performed a ring down experiment with no forcing. The resultant trajectory exhibited geometric decay for a significant range of angles about the bottom fixed point, which would suggest a frictional model for damping (see Figure 9). This is a result of the constant decrease in energy that occurs due to frictional decay. This constant

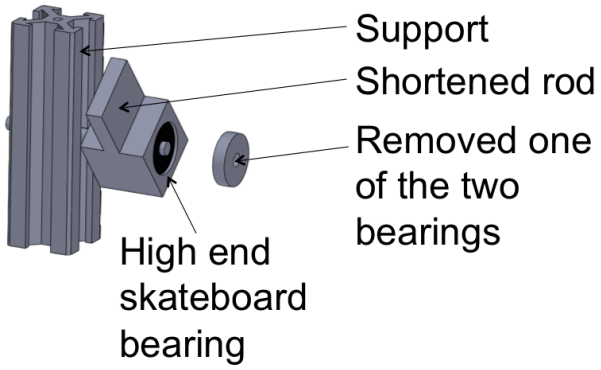

FIG. 8. Modified pendulum

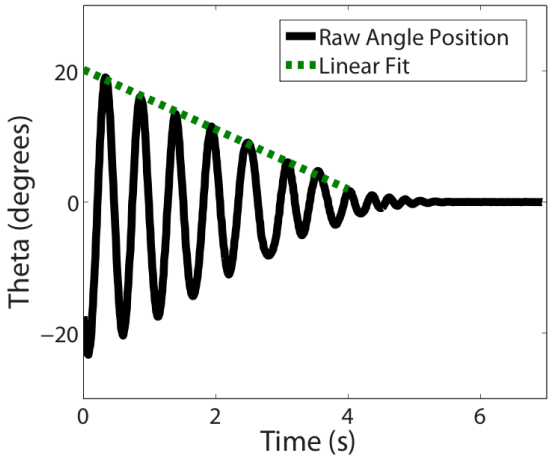

FIG. 9. Experimental ring down data at the bottom fixed point, no shaking

decrease causes the amplitude of oscillation to decrease by a constant value with every half swing[7]. And since the period of oscillation is estimated to be constant for small angles, the decay is expected to be nearly linear for frictional decay. Thus, a frictional damping model was used for simulations.

5. Lego Double Pendulum

The double pendulum was made from legos with equal effective lengths of 3.2 cm (see Figure 10). With no bearings, it exhibited no strange bearing issues, only even friction. Its axles of rotation were also plastic and would bend the entire pendulum in and out of the plane of rotation when significant forcing amplitudes were used. This added extra degrees of freedom and caused the occasional self-destruction of the pendulum. Yet, given more time, we discovered that an excellent pendulum could be designed out of mere legos!

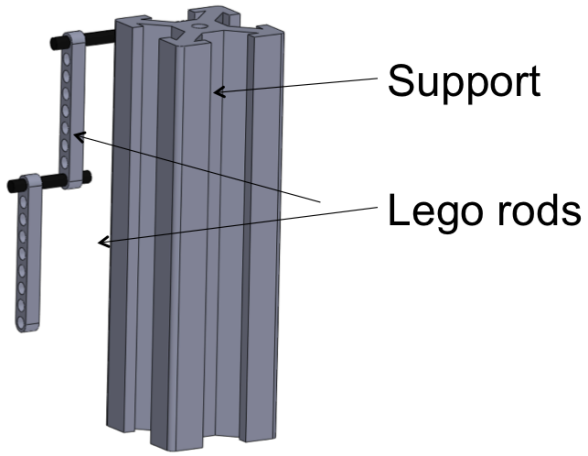

FIG. 10. Lego double pendulum

B. Procedure

1. Stability Boundary Mapping

The steps for mapping the stability boundary of the single pendulum were as follows:

1. Set the driving frequency for the shaker.
2. Support the pendulum at some small displacement from the inverted position.
3. Slowly increase current on the amplifier until the inverted equilibrium stabilizes.
4. Determine forcing amplitude from V_{pk}.

Reduce the amplitude to zero and repeat for all frequencies possible.

2. Frequency of Oscillation

The frequency of oscillation about the top fixed point was determined for a range of frequencies and amplitudes in which the pendulum was stable at the top. For a given set of amplitude and frequency, the pendulum was perturbed, and the resulting oscillations were recorded on camera and tracked. Frequency of oscillation data was extracted from this tracking data.

3. General Dynamics Tracking

Qualitative overall dynamics of the pendula could be extracted from tracked marker data for different behaviours that were exhibited.

IV. RESULTS

A. Stability Boundary Mapping

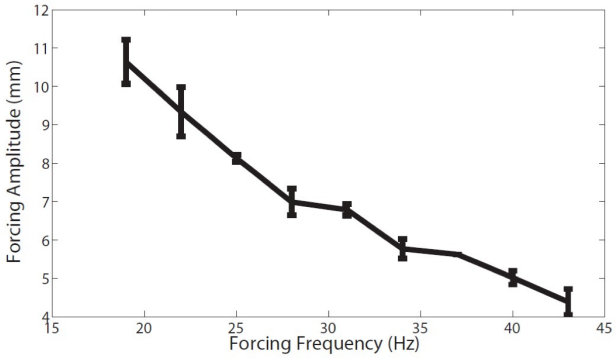

FIG. 11. Experimental results for stability boundary mapping. Error bars included represent standard deviation across 3 runs.

With the modified pendulum, we were able to slightly increase the range of frequencies to map out the stability boundary. Yet when comparing this result with the lower boundary in Figure 2, the data still looks nearly linear in comparison. However, upon determining f_0 from experimental ring down data, which was found to be approximately 1.87 Hz, we can then transform frequency and amplitude into the reduced units of Ω and ϵ, respectively. Superimposing this transformed experimental

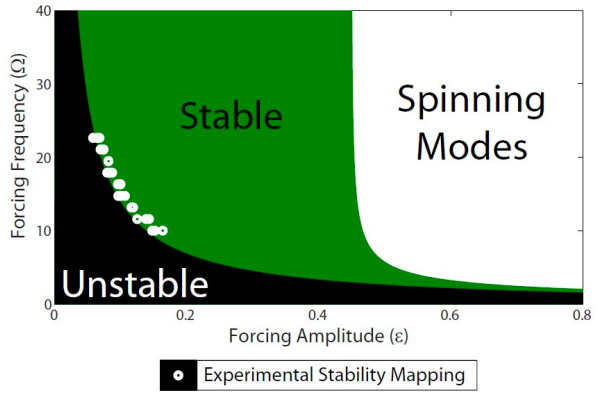

FIG. 12. Theoretical stability of inverted state with experimental mapping

data on the parameter space with the theoretical boundaries, it is clearly seen that, for our still relatively small range of frequencies, there is quantitative agreement between theory and experiment. Unfortunately, even with the improved pendulum, our constraints with the shaker and materials prevented us from fully exploring the parameter space.

B. Frequency of Oscillation

At forcing frequencies and amplitudes that stabilized the inverted pendulum, the pendulum was perturbed and tracked. It can be seen in Figure 13 that, while the damping dynamics are still affected very close to the fixed point, settling more consistently occurred at the fixed point instead of off-axis. With this oscillating data, frequency of oscillation was extracted for different forcing frequency/amplitude combinations. As the forcing amplitude increased, there was a positive correlation with the frequency of oscillation. In order to more broadly explore the effect of varying both forcing frequency and amplitude, I compared the frequency of oscillation with a proportional measure of the max kinetic energy exhibited by the shaker, which combined the forcing frequency and amplitude in the following way:

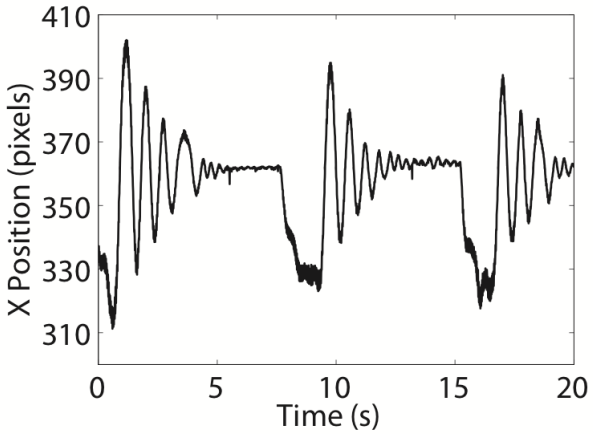

FIG. 13. Sample primary tracking data for the end tracker. Shaker forcing at 34 Hz and 6.5 mm

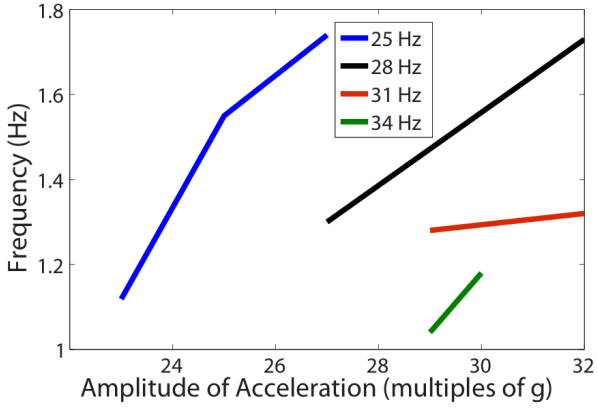

FIG. 14. Experimental frequency of oscillation vs forcing amplitude.

$$KineticEnergy/m = \frac{1}{2}(A2\pi f)^2 \qquad (12)$$

where m would be the mass of the moving parts in the oscillating base. The oscillation frequency seemed to

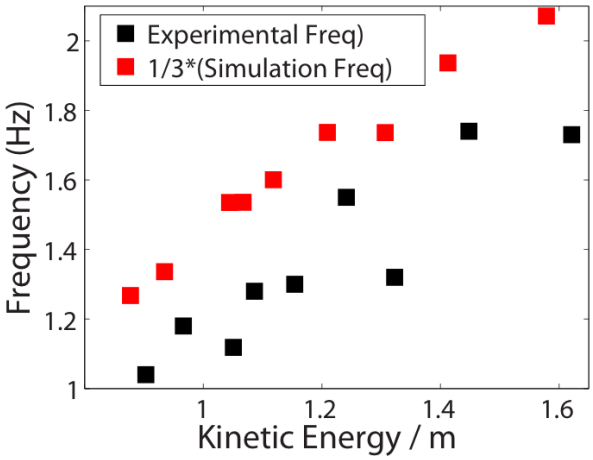

FIG. 15. Experimental and theoretical frequency of oscillation vs kinetic energy/m.

exhibit a fairly linear positive relationship with kinetic energy. This linear result was verified with simulation, which, while the scale of the results was larger than in experiment, still exhibited a definitively linear trend. Discrepancies in scale were likely due to a combination of the sensitivity of the oscillation frequency to the perturbation strategy as well as the strange friction issues we encountered with the single pendulum which may have slowed the oscillations during slow angular velocities.

C. Damping

While a frictional model of damping was decided, it is helpful to know what exactly γ is for our single pendulum simulation. Simplifying our equation of motion for the zero forcing ring-down scenario yields the following expression based on the small angle approximation:

$$\gamma = \pi^2 \frac{\Delta\theta_{max}}{T} \frac{1}{T} \tag{13}$$

where T is approximated as the constant period of oscillation. In the experiment, however, large amplitudes of oscillation occur, and small amplitudes are especially distorted due to strange bearing issues as well as resolution constraints. And thus, the above equation breaks down, and simulation output must simply be fit with experimental ring down data, such as the (x, y) pixel data of the end and pivot below. This data was transformed to θ based on the vector difference of pivot and end coordinates, and $\dot{\theta}$ was obtained by re-interpolating and differencing the θ time series. By tuning initial conditions and the natural frequency parameters, a fit for the friction coefficient, γ was established by varying the frictional parameter in Equation 3 and integrating the equation

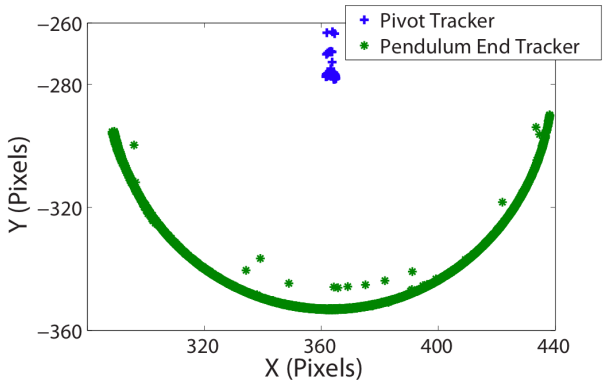

FIG. 16. Raw data of experimental ring down. No shaking.

until the RSME of the experimental and simulated time series was minimized. With this fit, γ was approximated

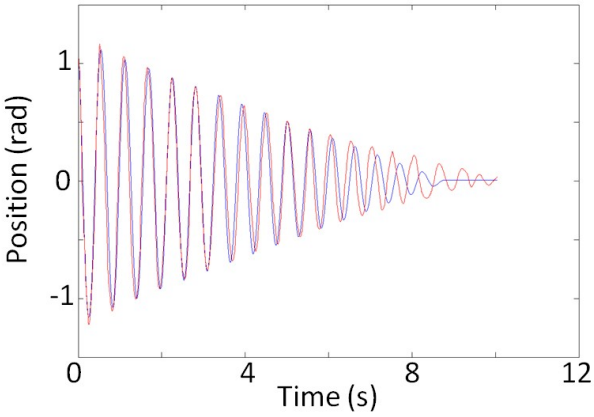

FIG. 17. Experimental vs theoretical ring down. Blue indicates integrated ring down; red indicates experiment.

to be 2.5.

V. DISCUSSION

A. Single Pendulum Dynamics

Further verification of experiment versus our simulation model is illustrated in Figure 18, in which both experimental and simulated phase portraits illustrate a successfully stabilized inverted pendulum with the same forcing parameters. Note the qualitative similarities in the behaviour of the trajectory in the phase plane as the pendulum dampens.

B. Double Pendulum Dynamics

We were able to successfully stabilize the double pendulum in both experiment and simulation, as illustrated

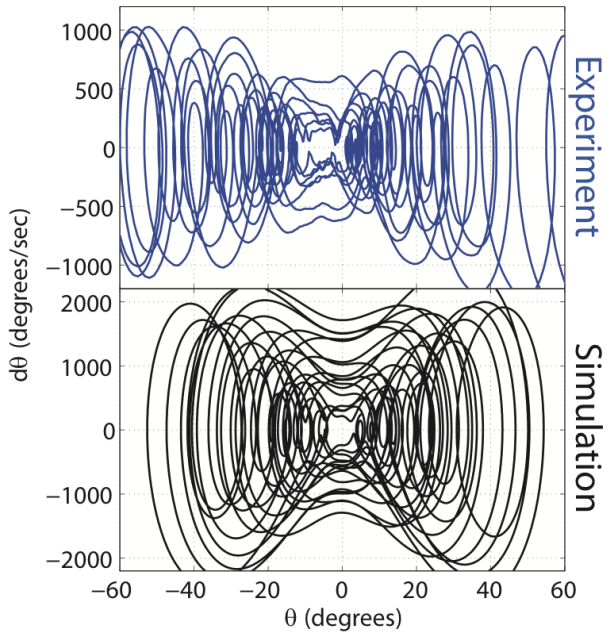

FIG. 18. Single Pendulum: Experimental vs simulated phase portraits at stable parameters: A = 10.7 mm, f = 25 Hz.

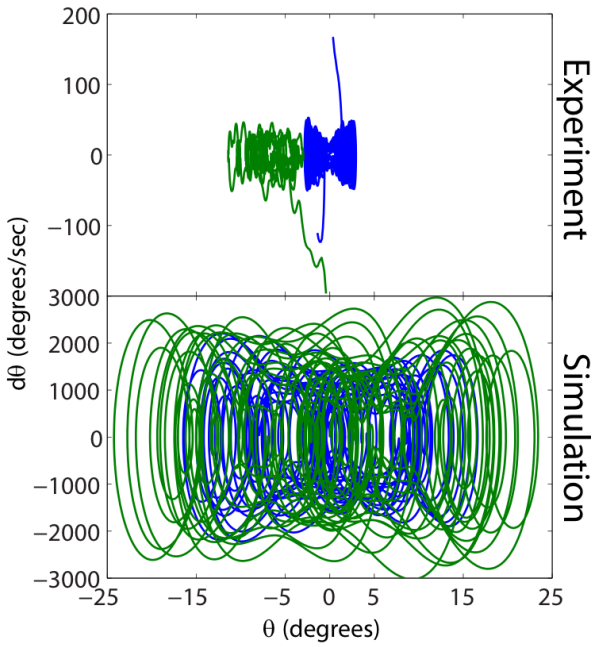

FIG. 19. Double Pendulum: Experimental vs simulated phase portraits at stable parameters: 30 Hz for experiment and 100 Hz for simulation. Blue trajectory is first pendulum; green is the second pendulum.

in Figure 19. However, the parameters for stabilization widely varied from experiment to simulation, and thus so did the behaviour of their trajectories in phase space. Since both pendula are dependant on each other, it should not very well be expected that one would be able to exactly recreate the trajectory of the double pendulum unless the initial conditions and forcing and pendula parameters are well known with high accuracy, which is not the case here. In this particular experiment, the second pendulum tended to only slightly oscillate about an angle just off-axis of the inverted position and did not cross zero degrees, while simulation showed oscillation about the inverted fixed point for both pendula.

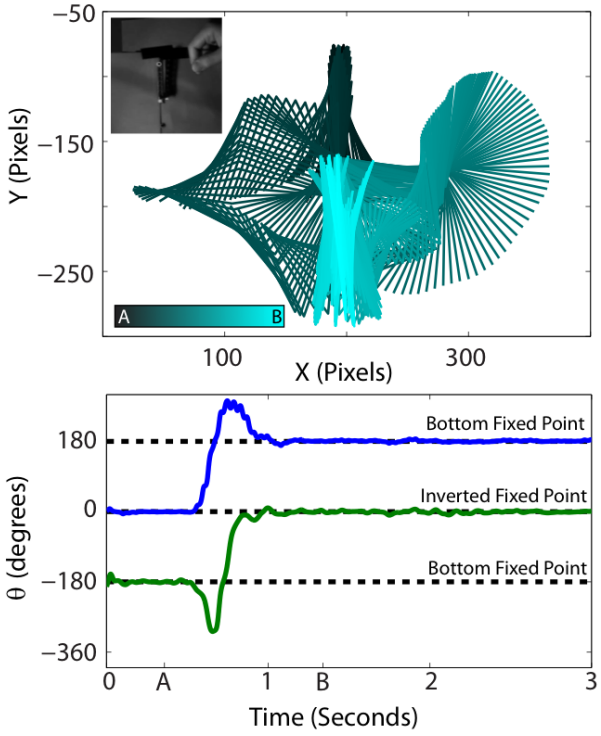

FIG. 20. Top: Illustration of the double pendulum configurations from time A to time B during a flipping motion. Bottom: Time series of the same flipping motion. Blue series is the first pendulum, and green is the second.

A striking behaviour that was periodically observed in the double pendulum was the separation of stabilizations. When the first pendulum stabilized at either the bottom or the top, the second pendulum could independently behave as a single pendulum would behave, giving rise to orientations in which one pendulum could be stable up and the other could be stable down, and vice versa, such as the flipping example in Figure 20, in which pendulum 1 and was initially stable up, and 2 was stable down. After a light flick perturbation, the entire pendulum flipped, as did the individual orientations.

C. Basins of Attraction

In the analysis of the stability of the inverted pendulum, it is instructive to see how the basins of attraction change when varying the forcing parameters. I was able to visualize these basins with the single pendulum Simulink model. The general method is to construct a

fine resolution array of initial states in the phase space and simulate the model at each of these initial states for a certain amount of time. For every point in this array, I assign a color corresponding to the final angular position of the pendulum. I employed the Interpolated Cell Mapping (ICM) algorithm to significantly accelerate the computation time[8]. This method only requires the simulation of the first forcing cycle at each initial state. And with this initial mapping, each initial state will be mapped to another initial state. And thus, one can iteratively interpolate through cycle by cycle for each initial state for any desired number of cycles. This method is many times faster than simply integrating the entire time trajectory at each point. Figure 21 shows a series of basins evolving for a 2.72 cm pendulum as the forcing amplitude increases from 0 to 1 cm.

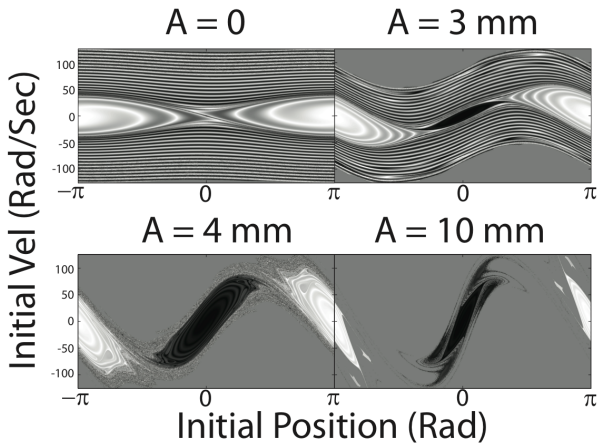

FIG. 21. Basins of attraction for increasing amplitudes. f = 50 Hz.

A black pixel corresponds to a set of initial angular position and velocity that settles at the inverted state. And white corresponds to settling at the bottom fixed point. Large expanses of grey indicate initial states that eventually mapped out of the phase space where no mapping was initially made, and thus could not be mapped further, even if the trajectory eventually returned. Stripes and noise indicate spinning modes that have yet to settle.

In determining where these forcing parameters would lie in Figure 2, a 50 Hz forcing amplitude with a 2.72 cm rod length would place the frequency in terms of Ω at approximately 25 based on the natural frequency. The ϵ coordinate travels from left to right as A increases. It is evident in Figure 21 that at $A = 0$, the inverted pendulum is still in the unstable region. By $A = 3$, the pendulum has passed the lower stability boundary as defined by Equation 4. As the amplitude continues to increase and approaches the second stability boundary defined by Equation 5, the inverted basin of attraction initially begins to dilate, and then elongates and becomes thinner. As this is happening, both basins seem to be rotating and approaching a vertical configuration in the phase space. I suspect that both basins eventually become perfectly vertical and infinitely thin as they cross the threshold into the spinning modes regime.

VI. CONCLUSION

Our experiments with the inverted pendulum confirmed that a simple sinusoidal shaking of the pivot is able to stabilize the top equilibrium point. Within this region of stability, the frequency of oscillation seemed to exhibit an interesting linear correlation with the maximum kinetic energy exerted by the oscillating base which was confirmed with simulation. Previous literature calculated the existence of non-trivial boundaries that define the regions of stability, instability and spinning in the amplitude/frequency parameter space, which was verified with our experiments of stability boundary maps, if only for a small range of frequencies. The evolution of the shapes of the basins of attraction as amplitude increases provides an illuminating view of how the basins transition from one region to another as these non-trivial boundaries are crossed.

We verified that a frictional model of damping was the most appropriate model for our experimental setup. And as most variations of the pendulum likely use some sort of bearing or surface-to-surface contact, it may be the preferred model for consideration of damping in most pendula, at least for simulation purposes. It would be interesting to study how varying the friction affects the basins of attraction and the stability boundaries.

We also succeeded in stabilizing the double inverted pendulum in both simulation and experiment. An interesting find with the double pendulum was the existence of separable behaviour, in which the second pendulum was, to a certain degree, able to act as a single pendulum, once the the first pendulum stabilized. A more thorough exploration of this phenomenon in both experiment and theory may be interesting. An unexpected realization occurred with the construction of the double pendulum in that legos are potentially very excellent candidates for a legitimate pendulum setup. Perhaps future students may want to seriously consider legos if a pendulum project arises.

Despite the strange bearing issues and rickety construction of the double pendulum, there was a shocking amount of qualitative congruence between our experimental data and the integrations of the simplified and idealized equations of motion. This qualitative agreement should serve as a testament to the permanence and influence of the interesting dynamics found in the inverted pendulum.

REFERENCES

[1]P. Kapitza, "Dynamical stability of a pendulum when its point of suspension vibrates, and pendulum with a

vibrating suspension," Collected Papers of PL Kapitza **2**, 714, 726 (1965).

[2]R. Grigoriev, "Symmetry and control: Spatially extended chaotic systems," PHYSICA D , 140(3– 4):171–192 (2000).

[3]T. Yamakawa, "Stabilization of an inverted pendulum by a high-speed fuzzy logic controller hardware system," Fuzzy Sets and Systems **32**, 161–180 (1989).

[4]A. A. Gerry K.A. Kramer-F Vanderstiggel Lyons and S. Stubberud, "Control of inverted pendulum system using a neural extended kalman filter," in *Proceedings of the Fourth internation Conference on Autonomous Robots and Agents* (2009) pp. 392–397.

[5]G. G. M. Bartuccelli and K. Georgiou, "On the dynamics of a vertically driven damped planar pendulum," in *Proc. R. Soc. Lond. A*, Vol. 458 (2001) pp. 3007–3022.

[6]H. N. Gronbech-Jensen James A. Blackburn, "Stability and hopf bifurcations in an inverted pendulum," American Journal of Physics **60**, 903–907 (1992).

[7]. R. B. A. Marchewka, D. Abbott, "Oscillator damped by a constant-magnitude friction force," American Journal of Physics **72**, 477–483 (2005).

[8]B. Tongue and K. Gu, "Interpolated cell mapping of dynamical systems," Journal of Applied Mechanics **55**, 461–466 (1988).